Reprinted from COLD SPRING HARBOR SYMPOSIA ON QUANTITATIVE BIOLOGY
Volume XXXVI, 1971
Printed in U.S.A.

Structure of Tomato Bushy Stunt Virus: Three-dimensional X-Ray Diffraction Analysis at 30 Å Resolution

STEPHEN C. HARRISON*

Laboratory of Structural Molecular Biology, Children's Cancer Research Foundation Boston, Massachusetts

The design of small, spherical viruses (Caspar and Klug, 1962) raises two sorts of questions. The first concerns the polymorphism of protein in the viral coat: how different are the configurations of quasi-equivalent structure units? Which intersubunit contacts are conserved in the distinct but quasi-equivalent environments, and which are not conserved? The second concerns the packing of the nucleic acid and its role in assembly: how is a linear molecule accommodated in an icosahedrally symmetric shell? To what degree does the nucleic acid stabilize or determine a particular configuration for the protein?

Tomato bushy stunt virus (TBSV) is probably the most suitable of the small, spherical viruses for X-ray diffraction structure analysis and, hence, for approaching these questions. The virus has a particle weight of 9×10^6 daltons and comprises a single molecule of RNA (1.5×10^6), 180 protein subunits (41,000), and possibly about 12 subunits of a minor protein component (28,000) (Butler, 1970; Weber et al., 1970). Electron micrographs of negatively stained particles show morphological units, interpreted as dimers located on the 30 strict twofold and 60 local twofold positions of the $T = 3$ icosahedral surface lattice (*cf.* Fig. 4) (Finch et al., 1970). The units are thus arranged in rings of six and five. Additional density is present at the centers of the rings of five: this feature may correspond to the minor protein component (Finch et al., 1970; Butler, 1970). A description of a three-dimensional reconstruction of the negatively stained TBSV particle from electron micrographs appears in the paper by Crowther and Amos in this volume.

A polymorphic aggregate of TBSV protein, the so-called "small particle," is an RNA-free spherical assembly with an outer radius of about 100 Å (Leberman and Finch, 1970). Similar particles may also be prepared from turnip crinkle virus (TCV), a virus structurally identical to TBSV. Three-dimensional reconstruction from electron micrographs shows that the subunit packing in the TCV small particle is similar to the arrangement in the rings of five morphological units in TBSV (Crowther and Amos, this volume). The additional density on the fivefold axes is also present. Although it has been suggested previously that small particles might be cores in the intact virus (Klug et al., 1966a; Harrison, 1969), the recently established molecular weight of the subunit rules out this interpretation.

The radial distribution of density in the TBSV particle has been determined from the spherically averaged X-ray scattering by virus in solution (Harrison, 1969). The results, summarized in Fig. 1,

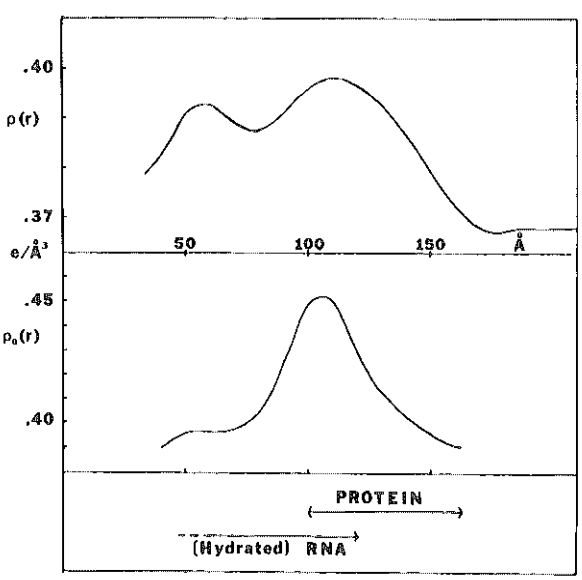

Figure 1. The radial organization of TBSV. *Top:* Radial electron density distribution in 1 M Na_2SO_4. The ordinate shows density in e/Å^3; the abscissa, distance (in Å) from the particle center. At any particular radius, the density is an average of solvent-containing regions ("holes") and solvent-excluding regions ("particle"). Outside the particle, the density is constant and equal to that of the solvent (0.368 e/Å^3). *Middle:* Electron density of solvent-excluding regions in the TBSV particle ("intrinsic electron density"), calculated from a comparison of radial electron-density distributions in several solvents. The curve terminates at the particle boundary. *Bottom:* Schematic interpretation of the radial organization.

* Present address: Department of Biochemistry & Molecular Biology, Harvard University, Cambridge, Massachusetts.

show a high "intrinsic electron density" (density of solvent-excluding regions) near a radius of 110 Å, with lower densities both inside and outside this shell. The peak at 110 Å represents a concentration of some part of the RNA. A radius of about 100 Å probably marks the inner boundary of protein in the intact virus, since the same subunits can form small particles with essentially identical packing. The most reasonable interpretation of the low intrinsic density at small radii ($r < 100$ Å) is to suppose that the rest of the RNA is coiled (perhaps somewhat irregularly) in the particle interior, with a particularly high degree of hydration. The amount of "bound" (solute-excluding) water required to produce this low density is about 1.5 g/g RNA—a rather high value but similar to the hydration of tRNA recently estimated by other methods (Kuntz et al., 1969; Tao et al., 1970). Tight binding of RNA to protein near 110 Å radius could account for the apparently smaller hydration of the RNA concentrated there.

TBSV Crystallography

TBSV forms body-centered cubic crystals (space group I23) with a unit cell edge length of 386 Å (Caspar, 1956). The orientation of icosahedral symmetry axes with respect to the crystal axes is shown in Fig. 2. Three-dimensional X-ray diffraction data have been collected to 16.5 Å resolution from crystals in three different solvents, 0.8 M and 4 M $(NH_4)_2SO_4$ and 1 M Na_2SO_4. Projection data have been obtained from crystals in $(NH_4)_2SO_4$-sucrose and Na_2SO_4-sucrose solutions. The differences between intensities from crystals in any two solvents fall off with increasing diffraction angle and vanish at spacings smaller than about 20 Å. Moreover, the intensities of all reflections depend only on the solvent density, whether the contributing species be sulfate or sucrose. The results show that small molecules and ions in the liquid filling the crystal interstices can penetrate into the virus particle, but that the subunits themselves are not porous (Harrison, 1969).

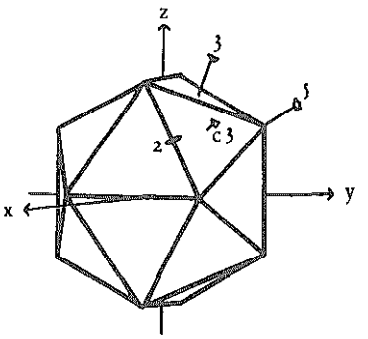

Figure 2. View of an icosahedron showing the orientation of symmetry axes relative to the axes of the cubic TBSV crystals. The numbers 5, 3, and 2 label non-crystallographic symmetry operations; C3 indicates a crystallographic threefold axis; x, y, and z are crystallographic dyads.

Figure 2 shows that some of the icosahedral symmetry axes (the [100] twofold axes and the [111] threefold axes) are also crystallographic axes, while others (the fivefolds and the remaining threefolds and twofolds) are symmetry operations of the particle but not of the entire crystal. The rotation function (Rossman and Blow, 1962) may be used to detect such non-crystallographic symmetry operations. Calculations (Table 1) show that the rotation-function peaks representing non-crystallographic icosahedral symmetry are equally strong using data from crystals in a high or a low density solvent, and the results in both cases are

Table 1. Peak Heights in the TBSV Rotation Function

Data set[a]	Origin peak[b]	Non-crystallographic dyad[c]	Background[d]
Native in 1 M Na_2SO_4	100	85	33
Native in 4 M $(NH_4)_2SO_4$	100	94	15
$PtCl_6^=$ Derivative in 1 M Na_2SO_4	100	78	34
Computed intensities from icosahedrally-symmetric model structure	100	81	36

[a] Three-dimensional data between spacings of 65 Å and 16.5 Å were included in the "large-term" rotation function computation. The maximum vector length was 150 Å in all cases.

[b] Results are shown normalized to a value of 100 for the self-interaction (rotation-function origin) peak. The Patterson origin peak has not been removed, and it contributes to the background.

[c] The peak heights indicated correspond to the non-crystallographic dyads, of which there is only one space-group independent set. The coordinates of the peak are $\kappa = 180°$, $\psi = 36°$, $\phi = 31°43'$.

[d] The background is the mean of values (away from the non-crystallographic dyad peak) along the line $\kappa = 180°$, $\phi = 31°43'$ in rotation-function space. The background varies along this line by no more than about ± 3.

comparable to the results with computed intensities from a perfectly icosahedral model structure. In the solvent of higher density, scattering at small angles from the protein subunits will be greatly weakened relative to that from the denser portions of the RNA, since the mean electron density of protein is about equal to the electron density of the solvent in question ($\rho_s \sim 0.41$ e/Å^3 in 4 M $(NH_4)_2SO_4$). The symmetry of ordered regions of RNA appears therefore to be as icosahedral at this resolution as the symmetry of the protein. Certain departures could, however, remain obscured by the distribution of particles over all possible icosahedral orientations in the crystal.

Pt Derivative

TBSV crystals soaked in solutions containing $PtCl_4^=$ or $PtCl_6^=$ (10^{-3} to 10^{-4} M) show similar strong intensity changes extending to at least 12 Å, the highest resolution examined (Fig. *3*). The soaking time required is a few hours in the case of $PtCl_4^=$, but similar differences with $PtCl_6^=$ appear only after several months. The intensity changes appear in both cases to be insensitive to washing the crystals with platinum-free mother liquor.

Three-dimensional data to 16 Å have been collected from $PtCl_6^=$-derivative crystals. Rotation-function calculations with native and derivative intensity data give no evidence that the introduction of $PtCl_6^=$ disturbs the icosahedral symmetry (Table 1). To scale native and derivative data sets, we make use of the centric [100] zone from a $PtCl_6^=$-soaked crystal immersed in a sucrose-containing medium of high electron density. The "Pt" and "Pt-plus-sucrose" data are scaled together using reflections beyond 1/20 Å^{-1}, which are independent of the solvent density. Native data in two different solvents are similarly treated. The scattering-amplitude differences at smaller angles, due to the solvent change, can then be compared for Pt-free and Pt-containing crystals. The two sets of differences are proportional as expected, showing that the addition of $PtCl_6^=$ does not produce changes in the solvent-excluding volume. A comparison of the four sets of data also permits identification of "crossovers"—terms that change sign in going from normal to high-density solvent or from native to Pt-derivative.

A statistical analysis of the Pt-induced intensity changes, using the methods introduced by Crick and Magdoff (1956), shows that the differences are too great to be due to isolated $PtCl_6^=$ groups. A comparison of centric and acentric reflections also indicates that the constellation of substituents is more centrosymmetric than the virus particle itself. These results suggest that $PtCl_6^=$ binds near symmetry axes: the resulting clusters of heavy atoms are not well resolved at 16 Å, and the intensity differences are significantly larger than those expected from an equal number of atoms more uniformly dispersed.

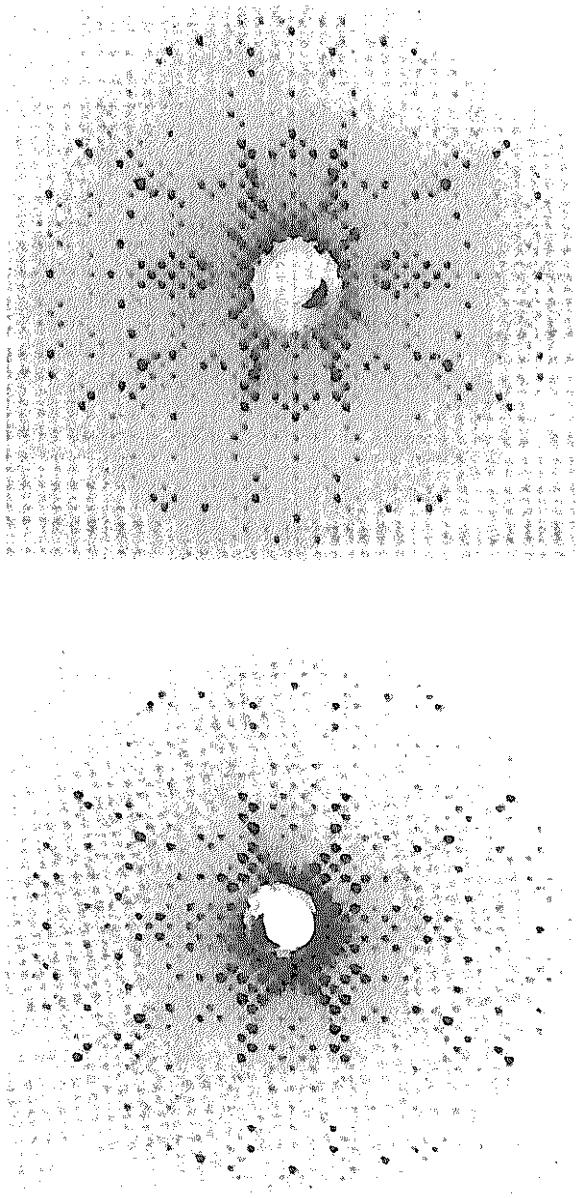

Figure 3. Precession photographs (3°) of the [100] zone of native (*top*) and $PtCl_6^=$-derivative (*bottom*) crystals of TBSV. The spikes of high-intensity reflections lie along icosahedral symmetry axes.

A three-dimensional $|\Delta F|^2$-Patterson synthesis has been computed, but the large number of overlapping peaks expected, even from a relatively small number of unresolved clusters, discourages interpretation. A stepwise approach to locating the heavy atom is suggested by the fact that the signs of the smallest angle reflections (out to

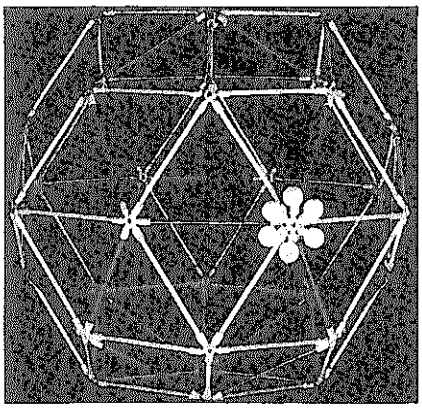

Figure 4. Skeletal model of a rhombic triacontahedron, illustrating the symmetry of a T = 3 icosahedral surface lattice. The edges of the lozenge-shaped faces (light rods) join fivefold and threefold (quasi-sixfold) axes, passing through quasi-twofold positions. The bisectors of these faces (dark rods) join two threefold vertices, passing through true twofold axes. The center of each triangle (half-face) is a quasi-threefold position.

The ring of six beads indicates the position of one cluster of six $PtCl_6^=$ ions in the TBSV derivative. Similar clusters should be imagined around the other threefold (quasi-sixfold) axes, all at about 112 Å from the center of the particle.

~50 Å) are known from the spherically averaged continuous transform (Harrison, 1969). A low-resolution difference Fourier shows strong peaks on the particle threefold axes (both crystallographic and non-crystallographic), at a radius of 110–115 Å. Trial structure-factor circulations give reasonable agreement ($R = 0.58$) to 25 Å resolution for the best coordinates. The approximate location of the heavy-atom positions are shown in a skeletal model in Fig. *4*. The major features of a Patterson map using calculated heavy-atom intensities correspond well to significant features in the $|\Delta F|^2$-Patterson. A difference Fourier synthesis at 25 Å resolution, based on phases from the trial coordinates, gives no clear evidence of additional sites.

In a T = 3 icosahedral surface lattice, particle threefold axes are quasi-sixfold in character, and locations near these axes are quasi-equivalent to positions near the particle fivefolds (Fig. *4*). The Pt binding gives clusters around the threefold (quasi-sixfold) axes but no substitution near the fives. This departure from chemical equivalence is important in view of the extra density on the fivefold axes seen in electron micrographs. Sites near the fivefold axes chemically identical to the binding positions near the threefolds could be blocked by the minor component or perturbed by the details of structure-unit packing.

Three-dimensional Structure

The Pt derivative gives signs for reflections in the real projection. To assess reliability of the phases, we have performed a three-dimensional reconstruction to a resolution of about 30 Å based on this one view. Such a computation is formally analogous to a three-dimensional reconstruction from an electron micrograph (*cf.* Crowther et al., 1970b). At 30 Å resolution, a single view is in fact not adequate for an accurate three-dimensional map, but the phased data from the real projection are supplemented by additional information: the position of nodes in the three-dimensional transform, given by reflections of unobservably small intensity, and signs for very small angle terms not in the *hk*0 plane but determined from the spherically symmetric part of the structure (Harrison, 1969). The effect of including these additional terms in the reconstruction has not been analyzed in detail, and the present map must therefore be regarded primarily as an assessment of the consistency of the positions determined for $PtCl_6^=$ ions with the external morphology of the virus particle known from electron microscopy. The view in question is centrosymmetric, and the resulting reconstruction will therefore necessarily have a center of symmetry. Since the T = 3 surface lattice is centrosymmetric, and since the distribution of mass at the outside of the TBSV particle is rather centrosymmetric (as revealed by negative staining: *cf.* Crowther and Amos, this volume), this limitation is probably not a severe one at the present resolution. That is, the resulting Fourier is a centrosymmetric average of a nearly centrosymmetric distribution.

The surface of a model based on this Fourier is shown in Fig. *5*. The model represents one octant of the spherical particle, viewed approximately along a quasi-threefold axis. The agreement with the results of electron microscopy (Finch et al. 1970; Crowther et al., 1970a) is in general excellent. Projections at the strict and local twofold positions indicate the clustering of protein subunits. These dimeric morphological units are sharper on the strict dyads (both crystallographic and non-crystallographic) than on the quasi-dyads, where they appear somewhat elongated in the direction joining the fivefold and threefold axes. This elongation is due in part to the fact that the density maxima on the quasi-twofold positions merge into less prominent but still significant bulges of density on the fivefold axes. They also spill over onto the particle threefold axes, but this density at outer radii along the threefolds conceals large cavities just within. The apparent threefold bulge is therefore likely to be an artifact of supplying somewhat insufficient data for the reconstruction. There are deep indentations on quasi-threefold positions.

An aspect of the packing of morphological units apparent on closer inspection of the model is an

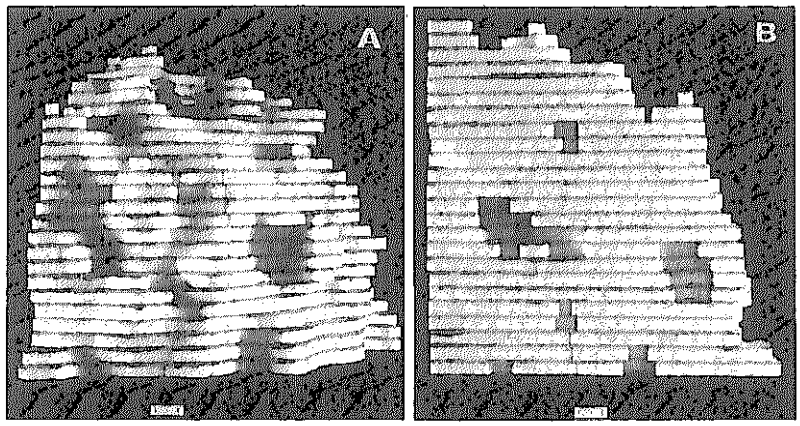

Figure 5. (A) Model based on one octant of the TBSV three-dimensional electron-density map. The view is approximately along a quasi-threefold axis, nearly identical to the views of an icosahedron in Fig. 2 and of a truncated icosahedron in Fig. 7. The interval between outer marks on the scale corresponds to 10 Å. (B) The xz plane of the same model. The view corresponds to a section through the particle and shows the cavities on the three and fivefold axes.

outward radial displacement of the tips of units on the quasi-dyads relative to the tips of those on the strict dyads. The difference in radii is between 5 and 10 Å, similar to the displacement observed in the three-dimensional reconstruction from electron micrographs (Crowther and Amos, this volume).

Internal Structure: RNA

Internal features in the density map are of two sorts: cavities of low density and rodlike regions of particularly high density. The major cavities are on the threefold axes near the outside of the particle and near the fivefold axes further within. The cavity on the threefold axis extends outward from a radius of about 110 Å. The $PtCl_6^=$ binding site is therefore located at the inner boundary of this region.

Several lines of evidence support identification of the regions of high density inside the particle with part of the RNA molecule. These features are confined to a radial shell around 110 Å. They correspond in detail to the only strongly positive density in a three-dimensional reconstruction using structure factors from TBSV in high electron-density solvent. In this second map, the contribution of protein structure units should be "matched out" by the medium. The second reconstruction ought to be more reliable than the first, since the only significant features are at smaller radii. The single view should therefore be more adequate for a proper determination of the three-dimensional density. A model based on this high solvent-density Fourier is shown in Fig. 6. It is a framework of somewhat flattened, rodlike features coinciding roughly with the edges of a truncated icosahedron (Fig. 7). These edges pass through the twofold and quasi-twofold positions of the $T = 3$ icosahedral surface lattice and intersect at the quasi-threefold positions. The sum of their lengths is about 4500 Å. This corresponds to between 20 and 30 per cent of the length of the TBSV RNA molecule, taking the nucleotide separation in TMV (5.2 Å; Caspar, 1963) and in a helix with stacked bases (3.4 Å) as upper and lower limits. Since the edges of the truncated icosahedron contain either a strict or a local twofold axis, the rodlike features in the Fourier probably correspond to two RNA chains.

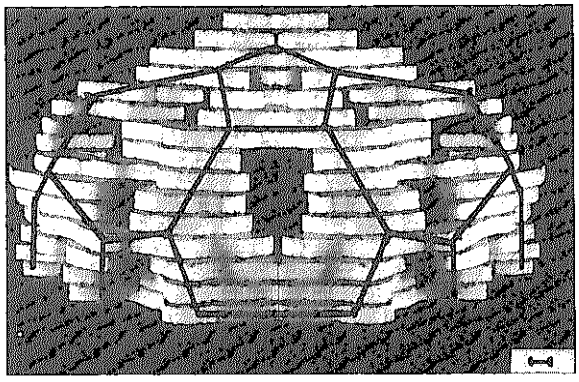

Figure 6. View down a crystallographic twofold axis of a model (two octants), based on a Fourier synthesis using structure factors from TBSV in high-density medium. The outline of a truncated icosahedron has been superposed on the picture. The large hole just above the direction of view surrounds a non-crystallographic threefold axis. Note that there is density at an inner radius on the crystallographic threefold; a feature, of density just below the cut-off contour, is present at a similar radius on the non-crystallographic threefold. Scale bar = 10 Å.

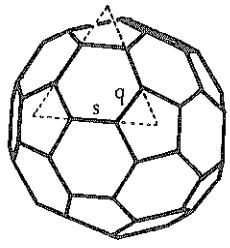

Figure 7. Truncated icosahedron viewed near a quasi-threefold position of a $T = 3$ surface lattice. The letters s and q indicate strict and local ("quasi") twofold positions respectively. The triangle shows one face of an icosahedron in the same setting.

The width of the density maxima, about 40 Å, also suggests that they represent more than one strand. The dyads and quasi-dyads do not, of course, require any bonding between the two chains, and it might be more reasonable to suppose a direct interaction of one piece of RNA chain with each protein subunit. This would account for 40 to 60 per cent of the TBSV RNA. The remainder is probably looped into such features as the bulges that mark quasi-threefold positions (Fig. 7) and into the center of the particle, producing the positive density at radii smaller than 100 Å (Fig. 1).

TBSV Assembly

The picture of TBSV that emerges from the present X-ray diffraction analysis and from the three-dimensional reconstruction from electron micrographs described by Crowther and Amos defines more precisely the questions raised in the introduction.

The most obvious difference between the morphological units on the strict and quasi-twofold axes is the relative outward displacement of the latter. The effect of this displacement on the local curvature at each dyad is shown in the photograph of a styrofoam-ball model of TBSV (Fig. 8). The surface at the strict dyad is almost flat: a morphological unit at this position lies in approximately the same plane as its four neighbors. By contrast, units on the quasi-dyads are at points of rather strong curvature. Two factors might contribute to this difference: the minor protein component on the fivefold positions and the RNA within. The similarity of the packing of morphological units in the small particles and on the quasi-twofolds suggests that, at least in the presence of the minor protein, the "natural" bonding pattern of the dimeric unit is the more sharply curved one. This curvature can give rise to the T = 1 particle, with an outer radius of about 100 Å. The interaction with RNA might be a factor in stabilizing the flatter bonding pattern of the dimers on strict twofold positions. The "flat" dimers can be thought of as linking the "curved" rings of five morphological units.

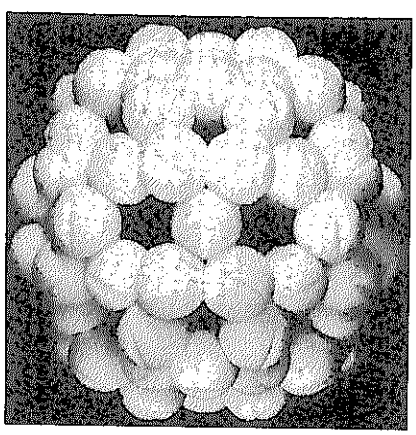

Figure 8. Model representing the arrangement of dimeric morphological units (styrofoam balls) in TBSV. The view is along a strict twofold axis. The units in the rings of five (e.g., just to the right and left of the direction of view) are all on quasi-twofold positions. Note that these units lie at somewhat larger radii than those on the strict dyads.

The arrangement of RNA in TBSV seems to preserve in considerable degree the T = 3 character of the protein shell. This observation suggests that nucleic acid is bonded in a similar or identical way to all 180 subunits. Both structural and chemical evidence indicates that in turnip yellow mosaic virus, RNA is also bound to each subunit (Klug et al., 1966b; Finch and Klug, 1966; Kaper, 1971). The protein-RNA interactions in these icosahedral viruses appear therefore to involve specific sites on the protein. Such specificity is known to characterize the bonding of RNA to protein in the helical tobacco mosaic virus, where the interaction is important in regulating assembly (Butler and Klug, 1971).

Acknowledgments

The author is indebted to Dr. D. L. D. Caspar for wisdom and encouragement and to Dr. R. A. Crowther for valuable criticism of the manuscript. The work was made possible by generous gifts of TBSV from Dr. C. A. Knight (Berkeley). Some of the X-ray data were collected by Mr. R. M. Lucas, whose assistance with photographic intensity measurement was also important. Thanks are due Mr. C. Ingersoll, Jr., for technical assistance, and Mr. Ray Fronk, for photography. The work was performed while the author was a Junior Fellow in the Society of Fellows, Harvard University. It was supported by PHS Grant CA-04696 (to Dr. Caspar) and by NSF Grant GB-25247.

References

Butler, P. J. G. 1970. Structures of turnip crinkle and tomato bushy stunt viruses. III. The chemical subunits: Molecular weights and number of molecules per particle. *J. Mol. Biol.* **52**: 589.

Butler, P. J. G. and A. Klug. 1971. Assembly of the particle of tobacco mosaic virus from RNA and disks of protein. *Nature New Biol.* **229**: 47.

Caspar, D. L. D. 1956. Structure of tomato bushy stunt virus. *Nature* **177**: 475.

——. 1963. Assembly and stability of the tobacco mosaic virus particle. *Adv. Protein Chem.* **18**: 37.

Caspar, D. L. D. and A. Klug. 1962. Physical principles in the construction of regular viruses. *Cold Spring Harbor Symp. Quant. Biol.* **27**: 1.

Crick, F. H. C. and B. Magdoff. 1956. The theory of the method of isomorphous replacement for protein crystals. I. *Acta Cryst.* **9**: 901.

CROWTHER, R. A., L. A. AMOS, J. T. FINCH, D. J. DE ROSIER and A. KLUG. 1970a. Three-dimensional reconstruction of spherical viruses by Fourier synthesis from electron micrographs. *Nature* **226**: 421.

CROWTHER, R. A., D. J. DE ROSIER and A. KLUG. 1970b. The reconstruction of a three-dimensional structure from projections and its application to electron microscopy. *Proc. Roy. Soc. London* A **317**: 319.

FINCH, J. T. and A. KLUG. 1966. Arrangement of protein subunits and the distribution of nucleic acid in turnip yellow mosaic virus. II. Electron microscopic studies. *J. Mol. Biol.* **15**: 344.

FINCH, J. T., A. KLUG and R. LEBERMAN. 1970. The structures of turnip crinkle and tomato bushy stunt virus. II. The surface structure: dimer clustering patterns. *J. Mol. Biol.* **50**: 215.

HARRISON, S. C. 1969. Structure of tomato bushy stunt virus. I. The spherically averaged electron density. *J. Mol. Biol.* **42**: 457.

KAPER, J. M. 1971. Studies on the stabilizing forces of simple RNA viruses. I. Selective interference with protein-RNA interactions in turnip yellow mosaic virus. *J. Mol. Biol.* **56**: 259.

KLUG, A., J. T. FINCH, R. LEBERMAN and W. LONGLEY. 1966a. Design and structure of regular virus particles, p. 158. *In* Principles of Biomolecular Organization (G. E. W. Wostenholme and M. O'Connor, ed.), Little, Brown & Co., Boston.

KLUG, A., W. LONGLEY and R. LEBERMAN. 1966b. Arrangement of protein subunits and the distribution of nucleic acid in turnip yellow mosaic virus. I. X-ray diffraction studies. *J. Mol. Biol.* **15**: 315.

KUNTZ, I. D., T. S. BRASSFIELD, G. D. LAW and G. V. PURCELL. 1969. Hydration of macromolecules. *Science* **163**: 1329.

LEBERMAN, R. and J. T. FINCH. 1970. The structures of turnip crinkle and tomato bushy stunt viruses. I. A small protein particle derived from turnip crinkle virus. *J. Mol. Biol.* **50**: 209.

ROSSMAN, M. G. and D. M. BLOW. 1962. The detection of sub-units within the crystallographic asymmetric unit. *Acta Cryst.* **15**: 24.

TAO, T., J. H. NELSON and C. R. CANTOR. 1970. Conformational studies on transfer ribonucleic acid. Fluorescence lifetime and nanosecond depolarization measurements on bound ethidium bromide. *Biochemistry* **9**: 3514.

WEBER, K., J. ROSENBUSCH and S. C. HARRISON. 1970. Structure of tomato bushy stunt virus. *Virology* **41**: 763.